BMC Gastroenterology

RESEARCH

Open Access

Vitamin D3/VDR alleviates double-stranded RNA virus -induced biliary epithelial cell damage by inhibiting autophagy

Na Liu[2†], Pu Zhao[3†], Ping Cao[4], JunPeng Hui[5], YongKang Pan[6] and Jiwen Cheng[1,4*]

Abstract

Background The increased apoptosis of bile duct epithelial cells (BECs) due to some damage factors is considered the initiating factor in the occurrence and progression of biliary atresia (BA). Vitamin D receptor (VDR) is thought to play a crucial role in maintaining the intrinsic immune balance and integrity of bile duct epithelial cells (BECs). To investigate the role of VDRs in the pathogenesis and progression of BA using in vitro and in vivo models.

Materials and methods The VDR expression levels in intrahepatic bile duct epithelial cells (IBDECs) in pediatric patients with BA were examined using immunohistochemical analysis. The correlation of the VDR levels with the incidence of refractory cholangitis after Kasai portoenterostomy (KPE) and the autologous liver survival time was analyzed. The levels of genes and proteins involved in related pathways were examined using quantitative real-time polymerase chain reaction and western blotting, respectively. The secretory levels of inflammatory factors were analyzed using enzyme-linked immunosorbent assay. A BA mouse model was established through the intraperitoneal sequential injection of rhesus rotavirus (RRV). The role of VDR in the pathogenesis and progression of BA was examined using in vitro and in vivo models. Retrospective analysis of patients with BA to examine the therapeutic efficacy of VDR activators on BA.

Results 15 pediatric BA patients exhibiting VDR downregulation in IBDECs showed a higher incidence of refractory cholangitis after Kasai portoenterostomy ($p=0.037$) and a lower native liver survival time compare to 23 BA patients without VDR downregulation ($p=0.032$). 1,25-VD3 inhibited the degree of autophagy induction in HIBECs by poly(I: C) ($p<0.05$), mitigated poly(I: C)-induced BEC damage and apoptosis by inhibiting autophagy ($p<0.05$). 1,25-VD3 significantly suppressed the poly(I: C)-induced downregulation of SRC ($p<0.05$) and ERK1/2 phosphorylation ($p<0.05$). 1,25-VD3 exert a protective effect against RRV-induced BEC damage by inhibiting autophagy in BA mouse model. The incidence of cholangitis and the native liver survival time after surgery in the calcitriol-treated group was significantly lower than that in the control group. ($p=0.033$, $p=0.035$, respectively).

[†]Na Liu and Pu Zhao contributed equally to this work.

*Correspondence:
Jiwen Cheng
chengjiwen68@163.com

Full list of author information is available at the end of the article

Conclusions VDR activator mitigated dsRNA-induced BEC damage and apoptosis by inhibiting autophagy in vitro and in vivo. The 1,25-VD3/VDR/Src axis alleviated poly(I: C)-induced HIBEC damage and apoptosis through the PLA2/PKC/ERK pathway.

Graphical abstract

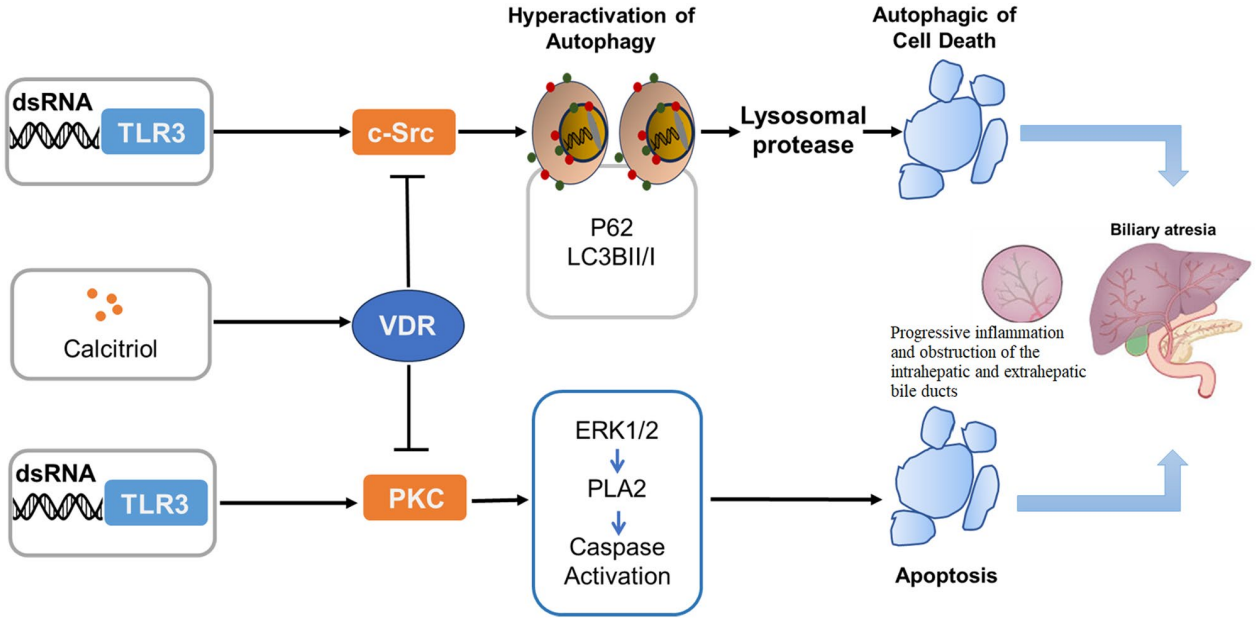

Keywords Biliary atresia, Vitamin D receptor, Biliary epithelial cell, Autophagy, Double-stranded RNA virus

Introduction

Biliary atresia (BA), which is characterized by progressive fibro-inflammation of the extrahepatic and intrahepatic bile ducts, may lead to cirrhosis and liver failure [1]. Kasai portoenterostomy (KPE) can restore bile drainage and remains the first choice of treatment for BA at present. Hormones, antibiotics, hepatoprotective agents, fat-soluble vitamins, and probiotics are often used to treat cholangitis and complications after KPE [1]. However, approximately 60% of patients develop liver failure after KPE and consequently require life-saving liver transplantation [1]. Currently, the etiology and pathogenesis of BA have not been elucidated, and effective strategies have not been developed to prevent progressive liver fibrosis postoperatively [2]. Therefore, the mechanisms involved in the occurrence and development of BA must be revealed. The early inhibition of BA progression can improve the prognosis of patients with BA.

In patients with BA, 1,25(OH)2D3 (1,25-VD3) deficiency is common due to the vitamin D activation disorder, and 1,25-VD3 deficiency is inversely correlated with liver fibrosis [3, 4]. Vitamin D receptor (VDR) knockout mice spontaneously develop hepatic fibrosis [5]. In the liver, VDR is mainly expressed in hepatic non-parenchymal cells such as hepatic stellate cells, sinus endothelial cells, Kupffer cells, and bile duct epithelial cells [6]. VDR plays an important role in maintaining the innate immunity of biliary epithelial cells (BECs) [7]. In mice, VDR deficiency in BECs disrupts cell junctions [8]. The apoptosis of intrahepatic bile duct epithelial cells (IBDECs) and extrahepatic bile duct epithelial cells is significantly upregulated in BA [9, 10] and is considered the factor initiating progressive liver fibrosis in BA patients [11, 12]. The roles of VDR in the occurrence and progression of BA and the underlying molecular mechanisms have not been previously reported. In this study, we examined the roles of 1,25-VD3 and VDR in the pathogenesis of BA along with the underlying mechanisms.

Results

The significant reduction of VDR expression in IBDECs may be a poor prognostic marker for BA

As shown in Fig. 1, VDR protein expression was localized to the cytoplasm of IBDECs with tan granular and diffusely distributed patterns (Fig. 1A). The mean immunohistochemical positive score of VDR in the IBDECs of children with choledochal cysts was approximately 3. Of the 38 pediatric patients with BA, 23 patients with a mean immunohistochemical VDR score ≥ 3 were classified into the "no-reduced VDR expression" (VDR-N)

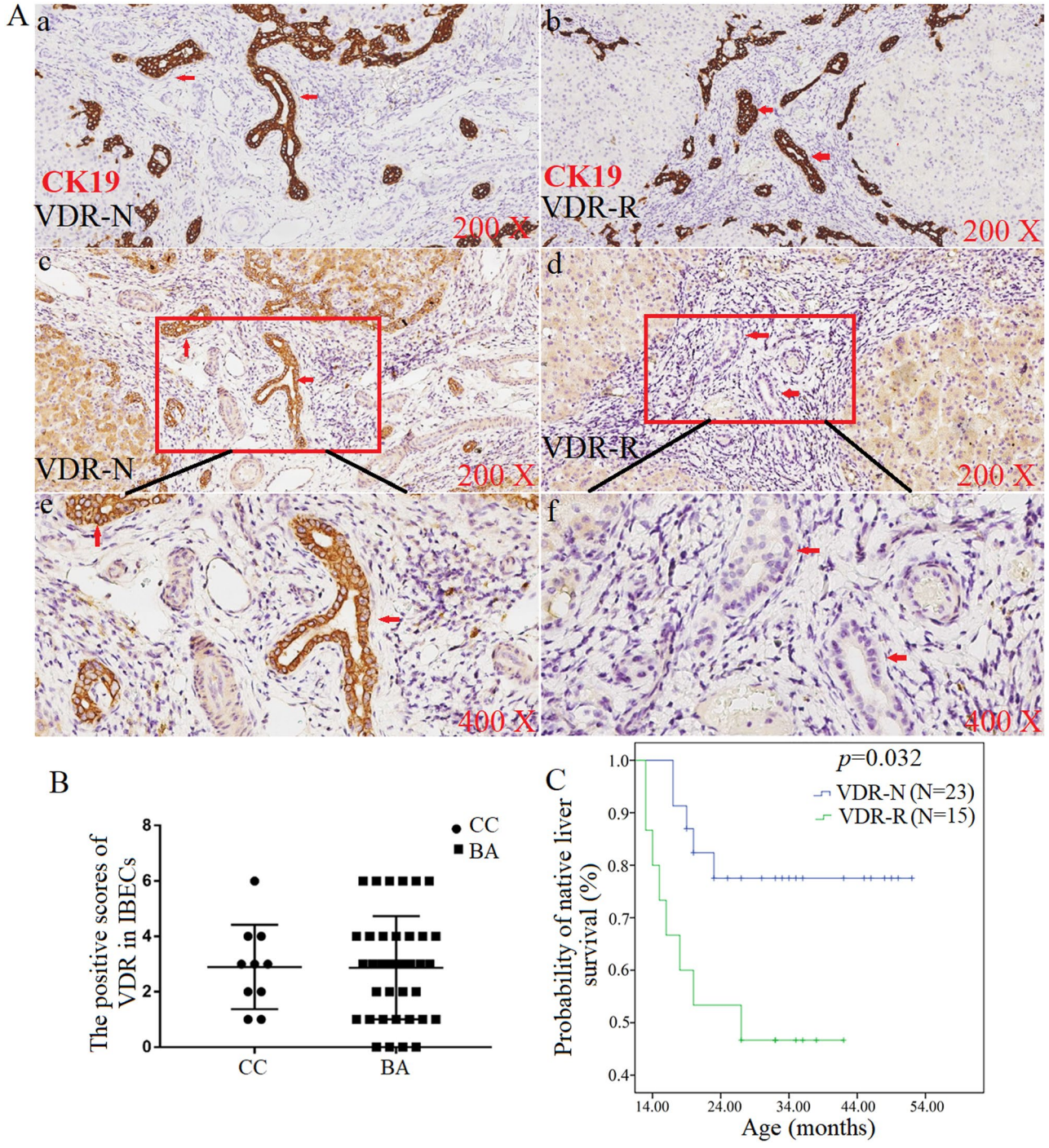

Fig. 1 A significant decrease in VDR expression in IBDECs may be a marker of poor prognosis in BA. (**A**) Panels a and b along with panels c and d represent consecutive sections of liver tissue from the same patients in the VDR-N and VDR-R groups. Panels a and b show immunohistochemical staining images of liver intrahepatic ducts labeled with CK19, corresponding to panels c and d. Panels c and d depict VDR immunohistochemical staining images of liver tissue from patients in the VDR-N and VDR-R groups. Panels e and f are magnified images of the regions outlined by red boxes in panels c and d, respectively, showing VDR staining in the epithelial cells of the intrahepatic ducts (indicated by red arrows). (**B**) The average expression level of VDR in the BA group compared with the CC group. (**C**) Curves of native liver survival in VDR-N vs. VDR-R group plotted using the Kaplan–Meier method. BA: biliary atresia; CC: choledochal cyst

group. Meanwhile, 15 patients with a mean immunohistochemical VDR score of < 3 were classified into the VDR-R group (Fig. 1B). Patients in the VDR-R group were associated with an increased rate of cholangitis ($p = 0.037$; Table 1) and decreased native liver survival time after KPE ($p = 0.032$, Fig. 1C). The clinicopathological characteristics of the patients were retrieved from their clinical records and are shown in Table 1.

Poly(I: C) promoted HIBEC damage and apoptosis by inducing autophagy

Poly(I: C) induced autophagy in HIBEC in a concentration-dependent manner. The level of autophagy induced by poly(I: C) at a concentration of 5 μg/mL was comparable to that induced by higher concentrations (Fig. S1); thus, poly(I: C) at a concentration of 5 μg/mL was used in subsequent experiments. The induction of autophagy in HIBEC by poly(I: C) was time dependent (Fig. 2A). Chloroquine (an inhibitor of autophagy) mitigated the poly(I: C)-induced downregulation of P62/SQSTM1, an autophagy-related protein (Fig. 2B). Consistently, cotreatment with chloroquine and poly(I: C) significantly decreased the formation of RFP-LC3 puncta, indicating that chloroquine mitigated poly(I: C)-induced autophagy ($p < 0.05$; Fig. 2C, D), further demonstrating that chloroquine mitigated the poly(I: C)-induced autophagy of HIBECs. Notably, poly(I: C) promoted apoptosis and inhibited the activity of HIBECs, whereas chloroquine suppressed the poly(I: C)-induced upregulation of apoptosis ($p < 0.01$, Fig. 2E, F) and inhibition of cell activity ($p < 0.01$, $p < 0.01$, Fig. 2G). Chloroquine also suppressed the poly(I: C)-induced secretion of inflammatory cytokines, such as INF-β, TNF-α, and IL-6 ($p < 0.01$, $p < 0.05$, $p < 0.01$, respectively, Fig. 2H, I, J). These findings suggest that poly(I: C) induced HIBEC damage and apoptosis by promoting autophagy. The autophagy inhibitor mitigated poly(I: C)-induced HIBEC injury and apoptosis by suppressing autophagy.

Table 1 The correlation between VDR and the clinicopathology of BA patients

Clinicopathological feature	VDR-*R* (15)	VDR-*N* (23)	*P* value
Female/male	10/5	16/7	1.000
Age at KPE (days)	61.56 ± 16.77	60.97 ± 17.56	0.950
C-reactive protein (mg/L)	45.2 ± 12.7	24.97 ± 12.15	0.092
WBC (× 10^9/L)	17.46 ± 7.13	12.49 ± 4.37	0.089
TBIL (mg/dL)	9.7 ± 3.2	8.8 ± 2.7	0.653
DBIL (mg/dL)	6.5 ± 2.0	6.1 ± 1.8	0.751
ALT (U/L)	216.5 ± 44.6	182.9 ± 41.2	*0.003*
AST (U/L)	168.8 ± 32.5	136.7 ± 28.5	*0.005*
Refractory cholangitis (yes/no)	9/6	5/18	*0.037*

WBC, White blood cells; CRP, C-reactive protein; TBIL, total bilirubin; DBIL, direct bilirubin; AST, aspartate aminotransferase; ALT, alanine aminotransferase

1,25-VD3 mitigated dsRNA-induced BEC damage and apoptosis by inhibiting autophagy

Poly(I: C) significantly downregulated VDR expression in HIBECs. As the treatment concentration of 1,25-VD3 increased, the decreased expression of VDR in HIBECs caused by poly(I: C) was gradually restored, demonstrating that 1,25-VD3 suppressed the inhibitory effect of poly(I: C) on VDR expression in a dose-dependent manner (Fig. 3A). Compared with the control group, poly(I: C) significantly increased the expression ratio of LC3B II to LC3BI in HIBECs while significantly decreasing the expression of P62. As the treatment concentration of 1,25-VD3 increased, the above phenomena were reversed, suggesting that 1,25-VD3 can inhibit the degree of autophagy induction in HIBECs by poly(I: C) in a concentration-dependent manner (Fig. 3B). 1,25-VD3 suppressed the autophagic flux in poly(I: C)-induced HIBECs ($p < 0.05$, Fig. 3C, D). The effects of poly(I: C) on the apoptosis ($p < 0.05$, Fig. 3E, F), cell viability (Fig. 3G), and the secretion of inflammatory cytokines were obviously reversed by 1,25-VD3 in a dose-dependent manner (IFN-β, $p < 0.05$, TNF-α, $p < 0.05$ and IL-6, $p < 0.05$, respectively, Fig. 3H, I, J). VDR activator mitigated dsRNA-induced BEC damage and apoptosis by inhibiting autophagy. Because the protective effect of 1,25-VD3 at 50 nM against poly(I: C)-induced HIBEC damage was like that of higher concentrations, 50 nM was used in subsequent experiments.

VDR knockdown suppressed the protective effect of 1,25-VD3 against poly(I: C)-induced HIBEC damage

1,25-VD3 upregulated VDR expression in poly(I: C)-treated HIBECs. To further confirm the role of VDR in poly(I: C)-treated HIBECs, HIBECs were transfected with si-VDR, pcDNA3.1-VDR, or the corresponding negative controls. Transfection with si-VDR and pcDNA3.1-VDR significantly downregulated and upregulated VDR expression, respectively ($p < 0.01$, $p < 0.01$, respectively, Fig. 4A). Next, HIBECs were transfected with si-VDR and subsequently treated with poly(I: C) and 1,25-VD3. VDR knockdown significantly mitigated the protective effects of 1,25-VD3 on the poly(I: C)-induced upregulation of apoptosis ($p < 0.05$, Fig. 4B, C), downregulation of cell activity ($p < 0.05$, Fig. 4D), and secretion of inflammatory factors in HIBECs (*IFN-β*, $p < 0.05$ *TNF-α*, $p < 0.05$ and IL-6, $p < 0.05$, respectively, Fig. 4E). Western blotting analysis indicated that VDR knockdown suppressed the inhibitory effect of 1,25-VD3 on poly(I: C)-induced autophagy, as evidenced by analyzing the numbers of red puncta in different treatment groups (Fig. 4F, G). This was further confirmed by the downregulation of P62/SQSTM1 (Fig. 4H, I). These findings indicate that VDR mediated the protective effects of 1,25-VD3 on poly(I: C)-induced HIBEC damage and apoptosis.

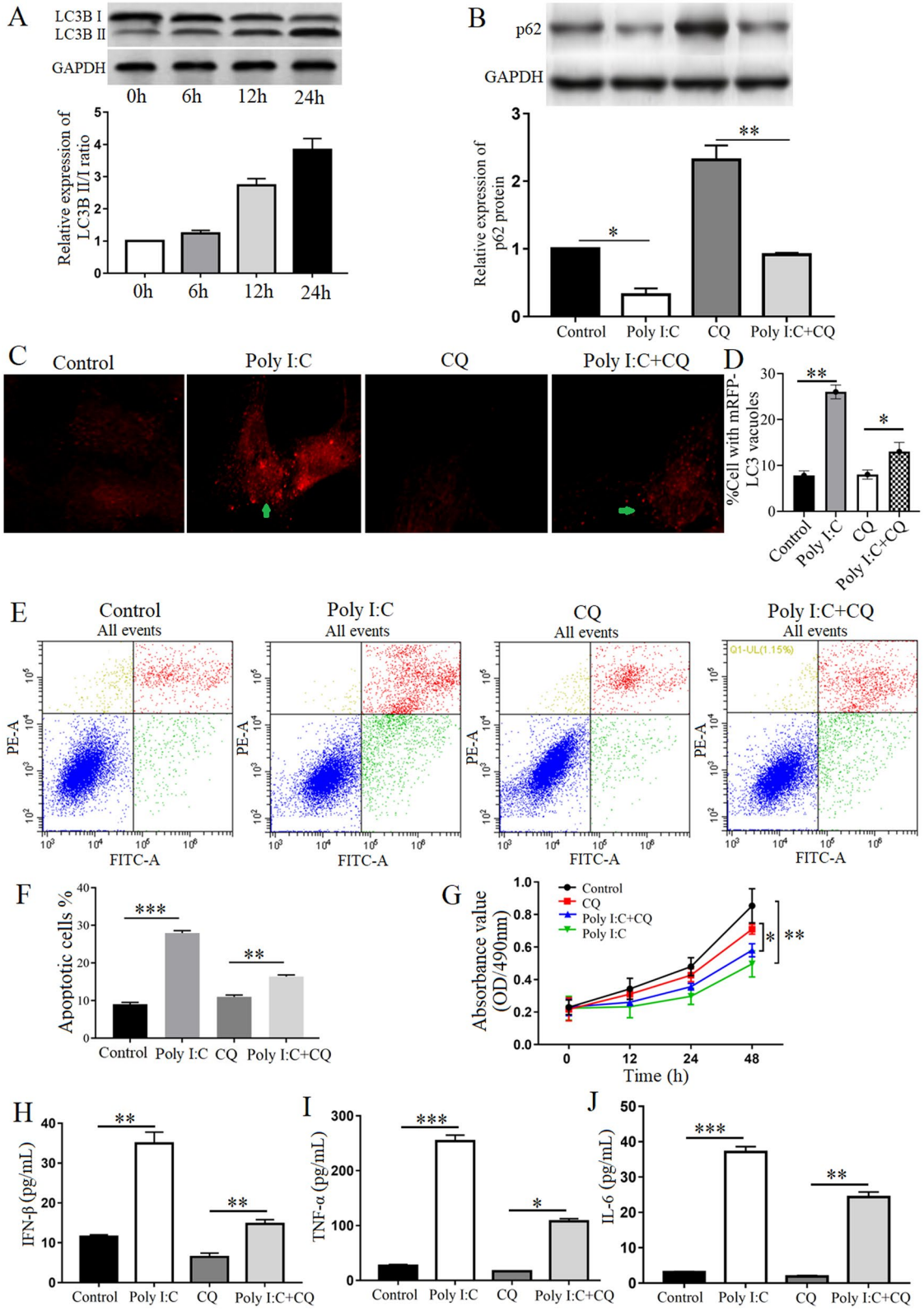

Fig. 2 (See legend on next page.)

(See figure on previous page.)

Fig. 2 Poly(I: C) promoted HIBEC damage and apoptosis by inducing autophagy (**A**) The relative expression levels of LC3B protein were detected by Western blotting in HIBECs treated with 5 μg/mL poly(I: C) for 0, 6, 12, and 24 h. (**B**) The relative expression of P62/SQSTM1 protein was detected by Western blotting. (**C**) Autophagic LC3 puncta were observed under fluorescent microscopy in mRFP-LC3B-transfected HIBECs for the indicated groups. (**D**) quantification of the number of LC3B puncta per cell from experiments in C. Bars represent the mean ± SEM of the number in 100 cells from 3 independent experiments. (**E**) The apoptosis rates in HIBECs subjected to different treatments were analyzed using flow cytometry. (**F**) quantification of the apoptosis rates in HIBECs from experiments in E. Bars represent the mean ± SEM from 3 independent experiments. (**G**) HIBEC viability was assessed by MTT assay. (**H**) The concentration of IFN-β was evaluated using ELISA kits. (**I**) The concentration of TNF-α, was evaluated using ELISA kits. (**J**) The concentration of IL-6 was evaluated using ELISA kits. CQ: Chloroquine. *$p < 0.05$, **$p < 0.01$, ***$p < 0.001$

1,25-VD3 exerted a protective effect on poly(I: C)-induced HIBEC damage through the VDR/SRC and PLA2/PKC/ERK pathways

The molecular mechanism underlying the effects of VDR on poly(I: C)-induced autophagy in HIBECs was examined. CAV1 and SRC are thought to be involved in VDR signaling [13]. The interaction between VDR and SRC was examined through Co-IP assay. VDR protein was enriched in the plasma membranes immunoprecipitated with anti-c-Src antibodies (IP-c-Src) (Fig. 5A, left panel). Meanwhile, SRC protein was enriched in the sample immunoprecipitated with anti-VDR (IP-VDR) antibodies (Fig. 5A, right panel). HIBECs were treated with 1,25-VD3 and subjected to immunoprecipitation assay. As shown in Fig. 5B, SRC and p-Y419-SRC coimmunoprecipitated with VDR in the plasma membrane fractions isolated from 1,25-VD3-treated HIBECs. Subsequently, the expressions of Toll-IL-1 receptor (TIR) domain-containing adaptor molecule-1 (TICAM1, also called TRIF), TLR3, and VDR proteins were examined. VDR knockdown significantly suppressed the effects of 1,25-VD3 on the expressions of VDR, TRIF and TLR3 (Fig. 5C, D, E). The interaction between 1,25-VD3 and VDR results in the activation of PLA2 and PKC downstream. Thus, the activities of PLA2 and PKC in HIBECs transfected with VDR siRNA and subsequently treated with poly(I: C) and 1,25-VD3 were examined. VDR knockdown partly mitigated the 1,25-VD3-induced upregulation of PLA2 and PKC activity ($p < 0.05$, $p < 0.05$, respectively, Fig. 5F and G). Additionally, 1,25-VD3 significantly suppressed the poly(I: C)-induced downregulation of SRC and ERK1/2 phosphorylation. In contrast, transfection with si-VDR mitigated the effects of 1,25-VD3 on SRC and ERK1/2 phosphorylation ($p < 0.05$, $p < 0.05$, respectively, Fig. 5H, I, J).

VDR activators may provide an effective approach for the treatment of BA

The rate of jaundice was significantly lower in the RRV + 1,25-VD3 group than in the RRV group at day 12 after viral inoculation (100% in RRV group vs. 50% in the RRV + 1,25-VD3 group; Fig. 6A and B, left). None of the mice in the WT + RRV group survived more than 14 d, while 40% of the mice in the 1,25-VD3 + RRV group survived for more than 18 d (Fig. 6B, right). In the 1,25-VD3 + RRV group, no blockages were observed in the extra-hepatic bile ducts (Fig. 6C), and no obvious infiltration of inflammatory cells was found around the intrahepatic bile ducts (Fig. 6D). The TEM images showed that no obvious autophagosomes were observed in the EBDECs of the control group. In the RRV group, a small amount of autophagic vesicles appeared in the EBDECs at day 6, and more autophagic vesicles were observed at day 12. The mitochondria were extremely swollen, and the crista process was disorganized, broken, or missing in the EBDECs. Compared with the RRV group, the amount of autophagic vesicles at day 12 was significantly reduced in the RRV + 1,25-VD3 group (Fig. 6E). The TEM images revealed that RRV induced the autophagosomal encapsulation of mitochondria in the EBDECs, while 1,25-VD3 significantly inhibited the autophagy induced by RRV in EBDECs.

We conducted a retrospective analysis of patients with BA who received oral calcitriol after KPE. The incidence of cholangitis after surgery in the calcitriol-treated group was significantly lower than that in the control group (Table 2). Additionally, the native liver survival time was higher in the calcitriol-treated group ($p = 0.035$, Fig. 7). The clinicopathological characteristics of the patients with BA are shown in Table 2. Thus, we can conclude that VDR activators exert a protective effect against dsRNA virus-induced BEC damage by inhibiting autophagy. These findings indicate that VDR activator is a potentially effective therapeutic approach for BA.

Discussion

The etiology and pathogenesis of BA have not been elucidated. Previous studies have demonstrated that inflammatory and immune responses are involved in the pathogenesis of BA, with viral infection and genetic variation being the etiological factors [2]. In BA, the apoptosis and epithelial–mesenchymal transition of BECs are associated with dsRNA virus-induced impaired innate immune response [2]. The direct virus-induced damage of BECs and secondary autoimmune reaction-induced damage to BECs lead to the occlusion of bile duct, resulting in the development of BA and liver fibrosis [14].

Poly(I: C) is an authentic mimic of viral dsRNA that elicits immune responses in HIBECs [15]. In this study, poly(I: C) significantly promoted autophagy and inflammatory response in HIBECs, decreased HIBEC viability, and enhanced HIBEC apoptosis. Chloroquine, an

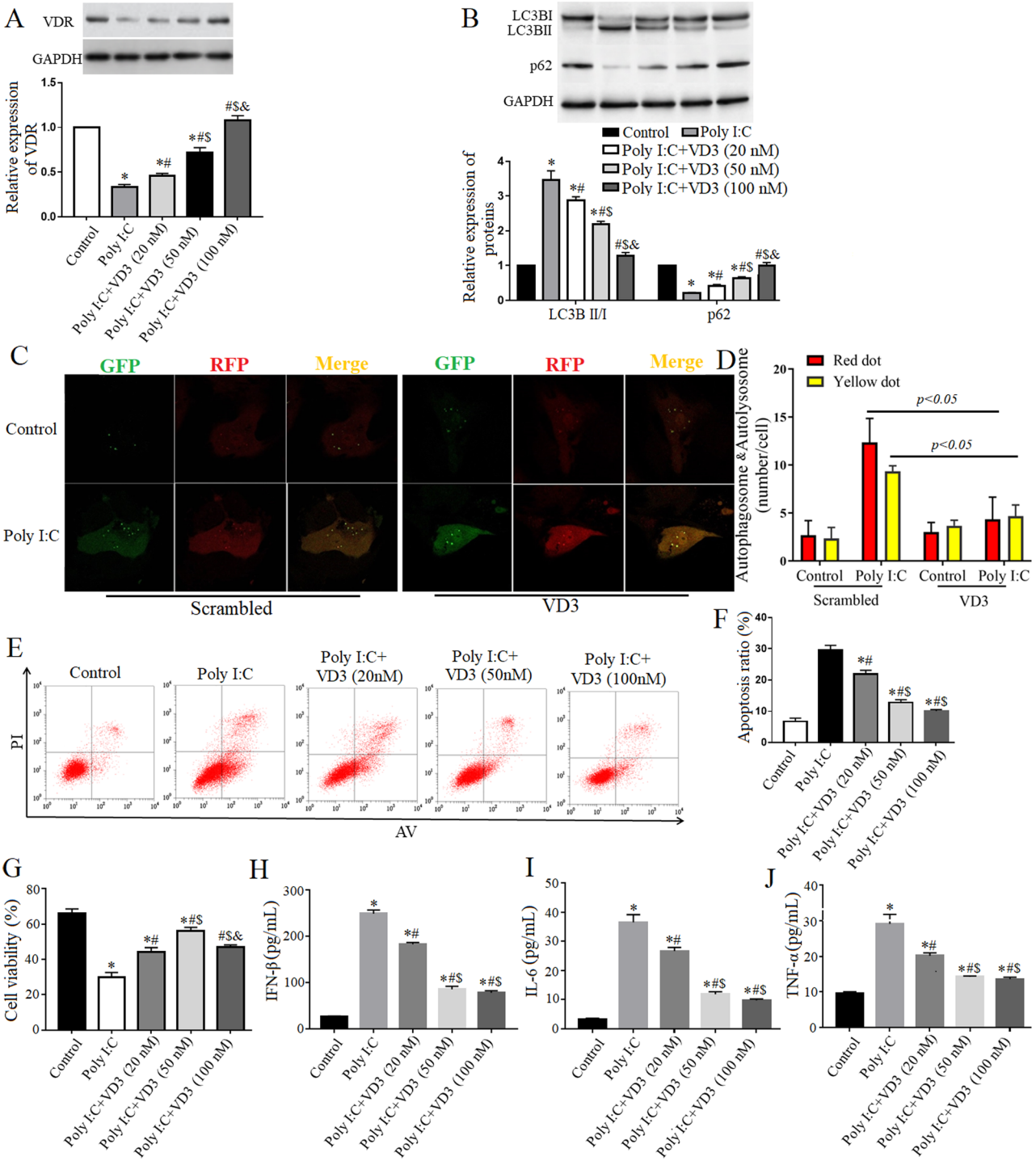

Fig. 3 Effects of 1,25-VD3 on cell autophagy, apoptosis, and inflammation induced by poly(I: C). HIBECs were incubated with 5 μg/mL poly(I: C) for 24 h followed by treatment with 1,25-VD3 (20, 50, or 100 nM) for 24 h. (**A**) VDR protein in the treated HIBECs was detected by Western blotting. (**B**) The relative expression levels of LC3B and P62/SQSTM1 proteins were measured in HIBECs exposed to different treatments. (**C**) HIBECs were transiently transfected with a plasmid encoding tandem GFP-mCherry-LC3B, and incubated with 5 μg/mL poly(I: C) or/and 50nM 1,25-VD3 for 48 h. The autophagosome is represented by a yellow dot with GFP and RFP, and the autolysosome is represented by a free red dot with RFP only. Scale bar: 10 μm. (**D**) Quantitative analysis of autophagosomes and autolysosomes in each cell. Bars represent the mean ± SEM from 3 independent experiments. (**E**) The apoptosis rates in HIBECs subjected to different treatments were analyzed using flow cytometry. (**F**) quantification of the apoptosis rates in HIBECs from experiments in E. Bars represent the mean ± SEM from 3 independent experiments. (**G**) HIBEC viability was assessed by MTT assay. (**H**) The concentration of IFN-β was evaluated using ELISA kits. (**I**) The concentration of IL-6 was evaluated using ELISA kits. (**J**) The concentration of TNF-α, was evaluated using ELISA kits. *$p < 0.05$ vs. the control group, $^{\#}p < 0.05$ vs. the poly(I: C) group, $^{\$}p < 0.05$ vs. the 20 nM group, $^{\&}p < 0.05$ vs. the 50 nM group

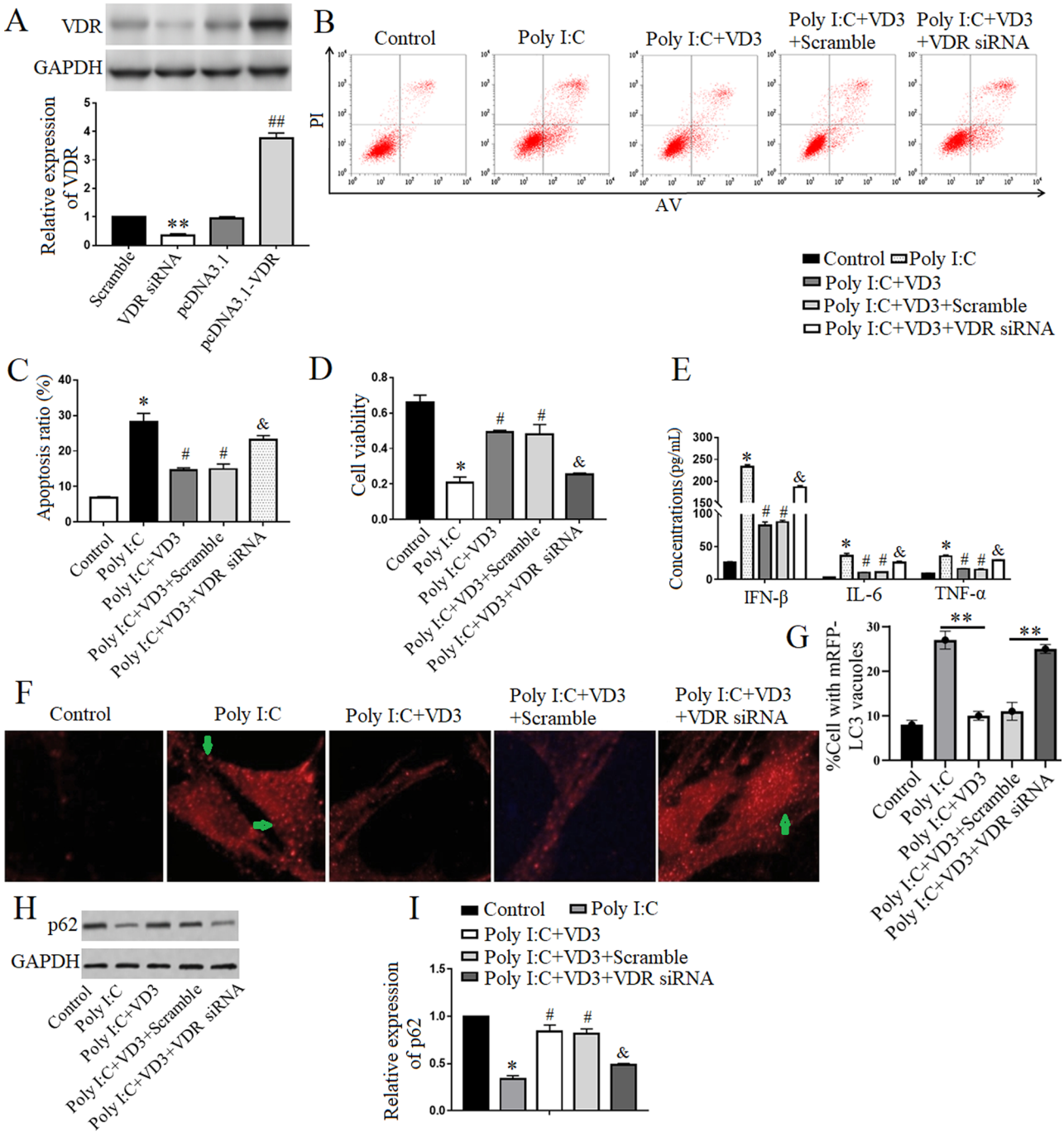

Fig. 4 Influence of VDR silencing on the protective effect of 1,25-VD3 in poly(I: C)-treated HIBECs. (**A**) VDR protein in HIBECs transfected with VDR siRNA, pcDNA3.1-VDR, or the corresponding negative control was detected by Western blotting. (**B**) The apoptosis rates in HIBECs subjected to different treatments were analyzed by flow cytometry. (**C**) quantification of the apoptosis rates in HIBECs from experiments in B. Bars represent the mean ± SEM from 3 independent experiments. (**D**) Cell viability was detected by MTT assay in HIBECs transfected with VDR siRNA followed by treatment with poly(I: C) and 1,25-VD3. (**E**) The concentrations of pro-inflammatory cytokines (IFN-β, TNF-α, and IL-6) were measured using ELISA kits. (**F**) Autophagic LC3 puncta were observed under fluorescent microscopy in mRFP-LC3B-transfected HIBECs for the indicated groups. (**G**) quantification of the number of LC3B puncta per cell from experiments in F. Bars represent the mean ± SEM of the number in 100 cells from 3 independent experiments. (**H**) The relative expression levels of P62/SQSTM1 protein were detected by Western blotting. (**I**) Quantification of P62 (normalized to GAPDH) from experiments as in H. The ratio of the indicated protein for control was arbitrarily set at 1. Bars represent the mean ± SEM from three independent experiments. $^{*}p < 0.05$ vs. the scramble or control group, $^{**}p < 0.01$, $^{\#}p < 0.05$ vs. the pcDNA3.1 or poly(I: C) group, $^{\#\#}p < 0.01$, $^{\&}p < 0.05$ vs. the poly(I: C) + 1,25-VD3 + scramble group

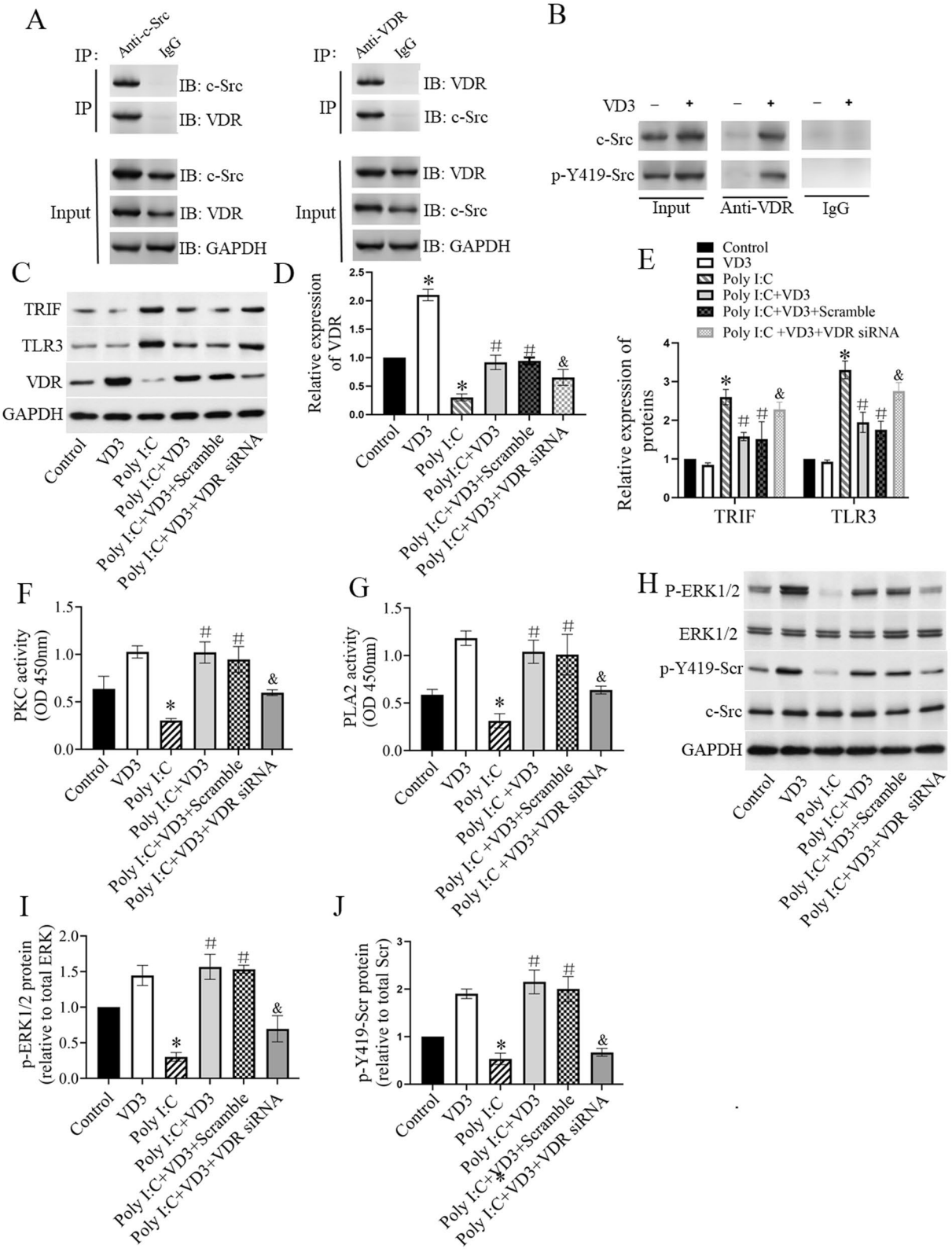

Fig. 5 (See legend on next page.)

(See figure on previous page.)

Fig. 5 VDR regulates poly(I: C)-induced autophagy in HIBECs via the PLA2/PKC/ERK pathway. (**A**) Co-IP assay of the interaction between VDR and c-Src. (**B**) HIBECs were incubated in the absence or presence of 1,25-VD3 (50 nmol/L), and the plasma membrane fraction was isolated. Co-immunoprecipitation against VDR was then performed. (**C**) The relative expression levels of TRIF, TLR3, and VDR protein were measured by Western blotting. (**D**) The levels of VDR (normalized to GAPDH) were quantified from experiments. The ratio of protein to GAPDH in the control group was arbitrarily set at 1. Data are presented as the mean ± SEM from three independent experiments as in C. (**E**) Quantification of TLR3 and TRIF (normalized to GAPDH) from experiments as in C. The ratio of the indicated protein for control was arbitrarily set at 1. Bars represent the mean ± SEM from three independent experiments. (**F**) PKC activity was evaluated using a PKC kinase activity assay kit. (**G**) PLA2 activity was analyzed using a cPLA2 activity assay kit. (**H**) The phosphorylation levels of c-Src and ERK were measured by Western blotting in different treatment groups. (**I**) Quantification of P-ERK1/2 (normalized to GAPDH) from experiments as in H. The ratio of the indicated protein for control was arbitrarily set at 1. Bars represent the mean ± SEM from three independent experiments. (**J**) Quantification of P-SRC-pY419 (normalized to GAPDH) from experiments as in H. The ratio of the indicated protein for control was arbitrarily set at 1. Bars represent the mean ± SEM from three independent experiments. $^{*}p < 0.05$ vs. the control group, $^{\#}p < 0.05$ vs. the poly(I: C) group, $^{\&}p < 0.05$ vs. the poly(I: C) + 1,25-VD3 + scramble group

inhibitor of autophagy, significantly suppressed poly(I: C)-induced autophagy, inflammation, and apoptosis in HIBECs. These results reveal that the pathological mechanism underlying poly(I: C)-induced apoptosis in HIBECs involves autophagy, and the inhibition of autophagy alleviates dsRNA virus-induced damage and apoptosis in HIBECs.

Autophagy plays an important role in maintaining the physiological functions of cells [16]. The dysregulation of autophagy can lead to ubiquitination inhibition, reactive oxygen species accumulation, mitochondrial dysfunction, increased genomic instability, and disrupted cellular homeostasis, thereby promoting the onset and progression of various diseases [16, 17]. Dysregulated autophagy can also help induce BEC senescence [18]. The markers of senescence (p53 and senescence-related β-galactosidase) are expressed in IBDECs of children with BA [19]. TEM revealed autophagic bodies in the IBDECs of pediatric patients with BA (Fig. S2). In patients with BA, the expression of P62 protein was significantly elevated in hepatocytes and IBDECs compared to children with choledochal cysts (Fig. S3). This suggests that autophagy dysregulation in BECs is a potential mechanism underlying BA pathogenesis. Autophagy has differential roles in different liver diseases. For example, autophagy induction exerts therapeutic effects in alcoholic hepatitis and nonalcoholic cirrhosis. Meanwhile, autophagy inhibition exerts therapeutic effects in liver fibrosis [20]. Thus, autophagy regulation may a potentially effective therapeutic strategy for BA.

Vitamin D activates autophagy through genomic and non-genomic signaling pathways, modulates various physiological functions of different organs, and regulates bone health and calcium metabolism [21]. Additionally, vitamin D is a natural agonist of VDR that induces autophagy as a protective mechanism to inhibit oxidative stress and apoptosis and, consequently, regulates cell proliferation, differentiation, and immune response [21]. For the first time, this study demonstrated that poly(I: C) promotes apoptosis and downregulates VDR expression in HIBECs. 1,25-VD3 exerted a protective effect against poly(I: C)-induced autophagy in HIBECs. Additionally, compared with the VDR-N group, pediatric patients with BA in the VDR-R group showed an increased frequency of cholangitis and a decreased native liver survival time after KPE. These results suggest that VDR downregulation in IBDECs may be a biomarker of poor prognosis in pediatric patients with BA. Hepatic VDR expression is markedly downregulated in patients with primary biliary cholangitis [22]. VDR plays an important role in maintaining the innate immunity of the bile duct epithelium [7]. A deficiency in VDR results in the loss of cell adhesion in BECs and disrupts bile duct integrity [8]. We speculated that dsRNA viruses induce BEC damage and apoptosis, significantly downregulate VDR expression, and promote bile duct damage, thereby contributing to poor prognosis in pediatric patients with BA who exhibit downregulation VDR expression in IBDECs.

In this study, 1,25-VD3 alleviated poly(I: C)-induced HIBEC damage by inhibiting autophagy in vitro, indicating that VDR activators are potential therapeutic agents for virus-induced BA. An RRV-induced BA murine model was used to verify the potential therapeutic effect of VDR activator on BA. 1,25-VD3 alleviated RRV-induced extrahepatic bile duct stenosis and intrahepatic inflammation in vivo. TEM revealed that 1,25-VD3 exerted a protective effect in extrahepatic BDECs by inhibiting RRV-induced autophagy. 1,25-VD3-induced autophagy is a protective mechanism that inhibits oxidative stress and apoptosis and regulates cell proliferation, differentiation, and immune response [23]. Vitamin D supplementation has been shown to have potential therapeutic effects in lupus animal models by modulating autophagy [24]. In intervertebral disc degeneration, VDR activation alleviates oxidative damage and suppresses nucleus pulposus apoptosis by promoting mitochondrial autophagy [25]. Sun et al. [3] reported that pediatric patients with BA show impaired vitamin D activation, and vitamin D deficiency is common and inversely correlated with liver fibrosis in BA patients. Calcitriol, an active metabolite of vitamin D and an agonist of VDR, has been used in the treatment of rickets in infants [26], demonstrating the basic safety of calcitriol in the treatment of pediatric diseases. After KPE, BA patients treated with calcitriol showed a

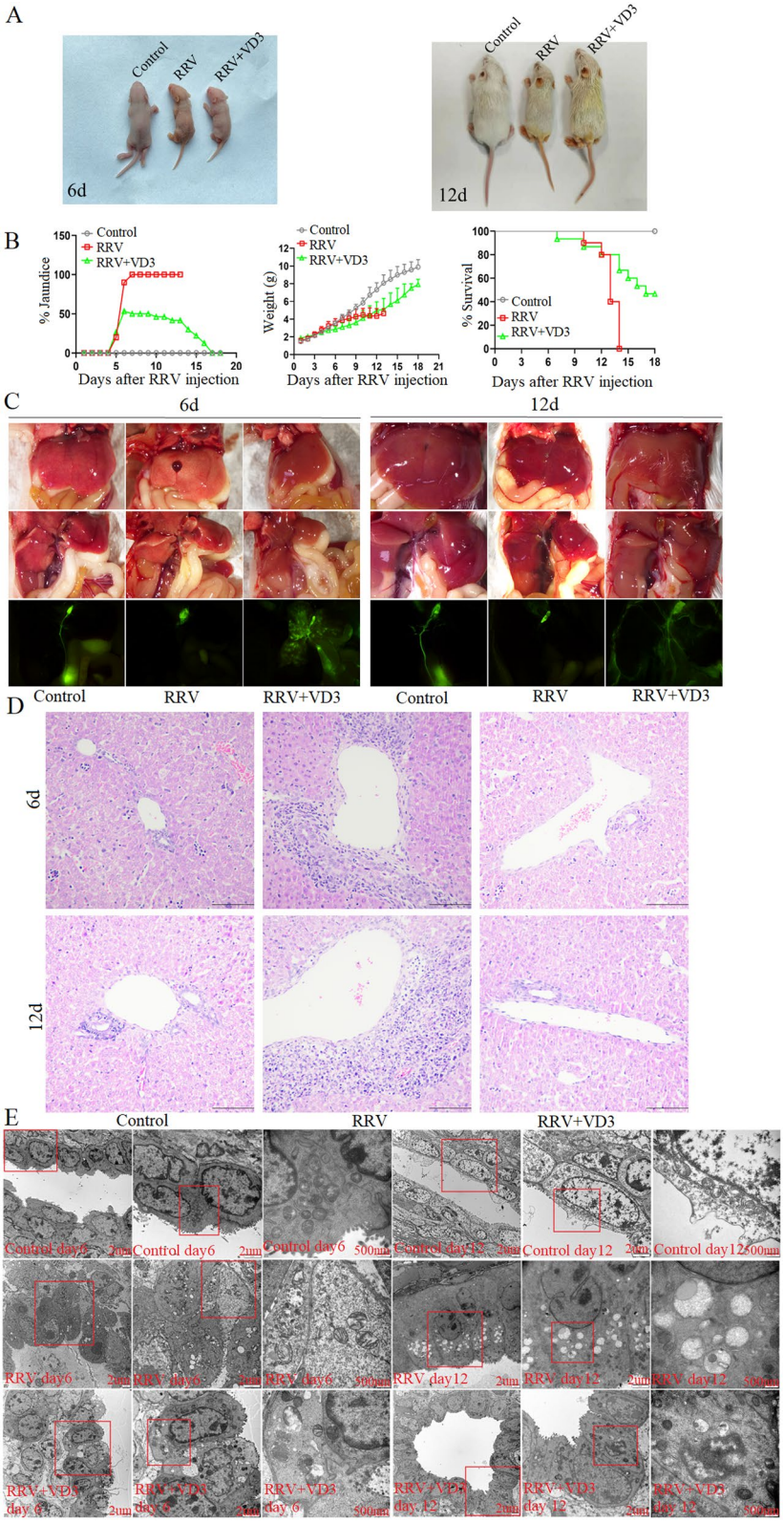

Fig. 6 Effects of 1,25-VD3 in mice infected with RRV. (**A**) Representative images of mice at days 6 and 12. (**B**) Jaundice rate (left), body weight curves (center), and survival curves of mice (right) recorded from days 1 to 20 in each group (control: WT + saline; RRV: WT + RRV; RRV + 1,25-VD3: WT + RRV + 1,25-VD3). (**C**) Extrahepatic bile duct cholangiography of mice in each group at days 6 and 12. (**D**) Liver H&E staining images for each group at days 6 and 12. (**E**) TEM images of autophagic vacuolization in EBDECs

Table 2 Basic clinical biochemical data for patients with biliary atresia according to group

	Control	Calcitriol	*P* value
	(*n* = 16)	(*n* = 14)	
Female/male	11/5	9/5	1.0
Age at KPE (days)	61.46 ± 17.57	60.67 ± 17.86	0.904
TBIL (mg/dL)	9.3 ± 2.3	9.0 ± 1.3	0.670
DBIL (mg/dL)	6.3 ± 1.7	6.0 ± 0.8	0.551
γ-GTP(U/L)	430.5 ± 100.3	371.8 ± 79.0	0.089
ALT (U/L)	101.5 ± 50.3	89.9 ± 41.5	*0.500*
AST (U/L)	149.5 ± 30.3	162.0 ± 49.7	*0.406*
VDR (R/N)	6/10	5/9	0.999
Refractory cholangitis(yes/no)	10/6	3/11	*0.033*

TBIL, total bilirubin; DBIL, direct bilirubin; AST, aspartate aminotransferase; ALT, alanine aminotransferase. γ-GTP, gamma-glutamyltranspeptidase

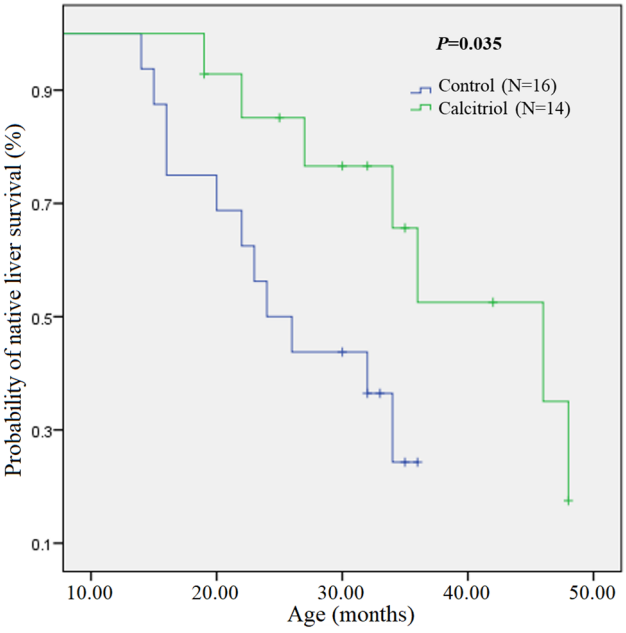

Fig. 7 Curves of native liver survival plotted using the Kaplan–Meier method according to whether calcitriol was taken orally

lower frequency of postoperative cholangitis, slower progression of liver fibrosis, and longer native liver survival time compared with untreated BA patients. These findings suggest that VDR activation is a potentially effective method for the treatment of BA.

In RRV-infected BECs, the expressions of pattern recognition receptors (e.g., Toll-like receptors) are upregulated, and the intracellular signaling pathways are activated, resulting in cell damage [27]. Poly(I: C), an extensively used immune stimulant, activates TLR3 ligand, induces an innate immune response, and upregulates TLR3 in BECs [28]. The lack of innate immune tolerance of poly(I: C) by TLR3 in BECs may contribute to the development of BA [28]. TLR3 mediates the host response against RNA virus through TRIF [29]. The TLR3 signaling pathway is dysregulated in TRIF-deficient or TRIF mutant mice [29], and TRIF overexpression can regulate the autophagy ubiquitination pathway [30]. This suggests that TRIF regulates TLR3 and autophagy ubiquitination. In this study, 1,25-VD3 mitigated the significant poly(I: C)-induced upregulation of TLR3 and TRIF3 in HIBECs. Meanwhile, VDR knockdown suppressed the beneficial effect of 1,25-VD3, suggesting that 1,25-VD3 activates VDR to regulate the autophagy ubiquitination pathway. 1,25-VD3 binds to VDR, which activates VDR-associated SRC to promote the release of the PDIA3/PLAA complex from CAV1 and subsequently PLA, thereby activating ERK1/2 [25]. This study also demonstrated that VDR knockdown suppresses the 1,25-VD3-induced upregulation of PLA2 and PKC activities and ERK1/2 phosphorylation. In summary, the 1,25-VD3/VDR/SRC axis mitigates poly(I: C)-induced HIBEC damage and apoptosis through the PLA2/PKC/ERK pathway.

This study has several limitations that must be addressed when considering clinical applications. First, this study only preliminarily demonstrated that the inhibition of autophagy can alleviate dsRNA virus-induced BEC damage and intrahepatic inflammation. The biliary atresia (BA) animal model used in this study cannot account for BA caused by cytomegalovirus infection or environmental toxins (such as biliatresone), which means the findings may not fully address damage caused by these other risk factors. Therefore, further studies are needed to determine the proportion of patients with BA who could benefit from clinical treatment with VDR activators. Second, the molecular mechanisms by which 1,25-VD3 alleviates cholangiocyte injury induced by RRV in animals and poly(I: C) in cells still need further verification to determine if they are consistent. Third, autophagy plays different roles in various liver diseases [20]. Promoting autophagy has potential therapeutic effects in alcoholic liver hepatitis and non-alcoholic liver cirrhosis, while inhibiting autophagy shows potential therapeutic effects in liver fibrosis and dsRNA virus-induced BEC damage. Our results did not reveal a significant correlation between the expression levels of VDR and P62 in IBDECs. Autophagy is a dynamic process, and its regulation may vary with the progression of the disease [31]. Thus, further clarification is needed to (1) determine which stage of autophagy is specifically affected by dsRNA virus-induced injury and bile duct epithelial cell apoptosis and (2) reveal the changes in autophagy levels at different stages of BA progression. These factors are crucial for treating BA through autophagy modulation. Therefore, much work is still needed to understand how to precisely modulate autophagy for the early-stage treatment of BA. Fourth, existing studies have shown that Vitamin D3/VDR can regulate inflammation and gut microbiota imbalance [32, 33], both of which may be contributing factors to the progression of BA. Whether

Vitamin D3/VDR exerts its effects through mechanisms other than the regulation of autophagy is worthy of further investigation. Fifth, chloroquine and hydroxychloroquine are well-known inhibitors of autophagy that are used to treat malaria (including neonates) and coronavirus disease in children [34]. However, the effectiveness of autophagy inhibitors in the early treatment of BA must be elucidated. Sixth, the number of pediatric patients BA included in this study was limited. Further large-scale randomized controlled trials are needed to validate the effects, optimal dosage, and duration of calcitriol administration for the treatment of BA. Finally, the prognosis of BA can be improved if the pathological process of BA can be blocked before extrahepatic bile duct obstruction. The effectiveness of VDR agonists in the early treatment of BA will be evaluated in future studies.

In conclusion, this study demonstrated that VDR downregulation in IBDECs is a marker of poor prognosis in BA patients. VDR agonists/activators are potential therapeutic agents for virus-induced BA. Furthermore, the 1,25-VD3/VDR/SRC axis alleviated poly(I: C)-induced HIBEC damage and apoptosis. The findings of this study provided novel insights for developing therapeutic interventions for BA.

Materials and methods

Human tissue specimens

In this study, 38 BA and 10 choledochal cyst liver tissue samples were collected from patients undergoing surgery at the Second Affiliated Hospital and Children's Hospital of Xi'an Jiaotong University between January 2015 and December 2019.

For clinical observation, 30 patients with BA who underwent KPE between January 2021 and June 2023 were recruited. Among them, 16 patients with BA were assigned to the control group, and 14 were assigned to the treatment group. The children in the control group received anti-inflammatory therapy (intravenous cefoperazone sodium and sulbactam sodium), hormone therapy [intravenous methylprednisolone (4 mg/kg/d for 2 weeks) and oral prednisolone (2 mg/kg/d for 2 weeks)], and oral vitamin D after KPE surgery. The patients in the treatment group received Rocaltrol (calcitriol) after KPE (0.25 μg, qod) instead of vitamin D until the hormone therapy was stopped. The remaining post-surgery adjuvant therapies in the treatment group were identical to those in the control group. The study was approved by the Ethics Committee of Xi'an Jiaotong University and informed consent (2020 – 660) was obtained from all patients and voluntary participation prior to the study.

Cell culture and treatment

Human intrahepatic BECs (HIBECs) were purchased from Jennio Biotechnology (Guangzhou, China) and cultured in Dulbecco's modified Eagle medium/Ham's F12 medium (1:1) supplemented with 10% (v/v) fetal bovine serum, 5 ng/mL epidermal growth factor, 0.4 μg/mL succinyl hydrocortisone, 2 nM triiodothyronine, 5 μg/mL insulin, 10 μg/mL recombinant human hepatocyte growth factor, 2 mM glutamine, 100 U/mL penicillin, and 100 μg/mL streptomycin at 37 °C in an atmosphere containing 5% (v/v) CO_2. HIBECs passaged 4–8 times were used in this study.

After reaching 75% confluency, the HIBECs were treated with 2.5–10 μg/mL poly(I: C) (Invitrogen, San Diego, CA, USA) for up to 48 h or with 5 μg/mL poly(I: C) for 24 h. Subsequently, the cells were treated with various concentrations of 1,25-VD3 for 24 h.

Cell transfection

The VDR overexpression vector (pcDNA3.1-VDR) and the control vector (pcDNA 3.1) were purchased from GenScript Biotech Corp. (Nanjing, China). Small interfering RNA (siRNA) against VDR (si-VDR) and its negative control (scramble) were purchased from ThermoFisher Scientific (Waltham, MA, USA). Plasmids and oligonucleotides were transfected into HIBECs using Lipofectamine 2000 transfection reagent (Invitrogen, Carlsbad, USA) following the manufacturer's instructions. At 48 h after transfection, the cells were harvested for further analysis.

Cell viability

Cell viability was analyzed by 3-(4,5-dimethylthiazol-2-yl)-2,5-diphenyltetrazolium bromide (MTT; Sigma, St Louis, USA) colorimetric assay. Briefly, cells were seeded in 96-well plates at a density of 5×10^3 cells/well and subjected to different treatment regimens. After treatment for the indicated duration, the cells were incubated with MTT solution (20 μL, 5 mg/mL; Sigma) at 37 °C for 4 h. The medium was then removed, and the sample was incubated with 0.1 mL of dimethyl sulfoxide (Sigma) to dissolve the formazan product. Subsequently, the absorbance of the reaction mixture at 450 nm was measured using a microplate reader (BioTek, Winooski, USA).

Cell apoptosis analysis

Cell apoptosis was examined using an annexin V/fluorescein isothiocyanate (FITC) and propidium iodide (PI) apoptosis detection kit (Becton Dickinson, USA) following the manufacturer's instructions. At 48 h after transfection, the HIBECs were suspended in annexin-binding buffer and incubated with annexin V-FITC/PI solution for 15 min in the dark at room temperature. The apoptosis rate was determined using flow cytometry (CYTOMICS FC 500, Beckman Coulter, USA).

Enzyme-linked immunosorbent assay (ELISA)

The secretion levels of interleukin (IL)-6, interferon (IFN)-β and tumor necrosis factor (TNF)-α were determined by commercially available ELISA kit (Enzo Life Science, Inc., Farmingdale, NY, USA) according to the manufacturer's protocol. Briefly, the culture supernatants were added to each well, incubated with the standard biotin solutions, absorbance was read at 450 nm using an ELISA reader (iMark microplate reader, Bio-Rad, Hercules, California, USA). The concentration of each cytokine was calculated by recombinant human polyclonal IFN-β, TNF-α and IL-6 standard curves.

Western blotting

Harvested cells were lysed for 30 min in radioimmunoprecipitation assay buffer (Sigma-Aldrich, St Louis, MO) supplemented with protease inhibitors. Total protein was extracted from the treated HIBECs using M-PER TM Mammalian Protein Extraction Reagent (ThermoFisher Scientific, Waltham, MA, USA). The extracted protein was quantified using a bicinchoninic acid assay kit (ThermoFisher Scientific, Waltham, MA, USA). The protein samples were subjected to sodium dodecyl sulfate-polyacrylamide gel electrophoresis, and the resolved proteins were transferred to a polyvinylidene fluoride membrane (Millipore, Billerica, MA, USA). The membrane was sectioned before antibody hybridization and was individually probed with the following primary antibodies overnight at 4 °C: anti-VDR (ab32042, 1:500), anti-P62/SQSTM1 (ab91526, 1:1000), anti-LC3B (ab48394; 1:400), anti-C-SRC (ab109381; 1:1000), anti-Y419-phospho-SRC (ab185617; 1:1000), anti-TRIF (ab13810; 1:1000), anti-TLR3 (ab137722; 1:1000), anti-ERK1/2 (ab17942; 1:1000), anti-p-ERK1/2 (ab214362; 1:1000), and anti-GAPDH (ab8245, 1:5000) antibodies. Next, each membrane was washed twice with PBS and incubated with goat anti-rabbit IgG HRP (1:2000; Santa Cruz, CA, USA) for 1 h at room temperature. Immunoreactive signals were visualized using enhanced chemiluminescence and quantified using Image J software (NIH, Bethesda, MD, USA). GAPDH was used as the loading control.

Detection of PKC activity

PKC activity was measured using a PKC kinase activity assay kit (Abcam). Briefly, the lysates of treated HIBECs were transferred to a PKC substrate microtiter plate and incubated with 10 μL of ATP at 30 °C for 2 h to initiate substrate phosphorylation. The sample was then incubated with a specific antibody against the phosphorylated substrate at room temperature for 1 h followed by incubation with horseradish peroxidase-conjugated secondary antibodies for 30 min. Immunoreactive signals were developed using tetramethylbenzidine. The reaction was terminated using the stop solution. The absorbance of the reaction mixture at 450 nm was evaluated using a microplate reader (BioTek, Winooski, USA). The PKC kinase activity was expressed as the optical density at 450 nm (OD_{450}).

Detection of PLA2 activity

The PLA2 activity was evaluated using a cPLA2 activity assay kit. After washing with PBS, cells were lysed to obtain the cell supernatant. The lysate was transferred to a microplate and incubated with arachidonoyl thiophosphatidylcholine at room temperature for 1 h (following the manufacturer's instructions). Subsequently, the sample was incubated with 5,5′-dithiobis (2-nitrobenzoic acid) for 5 min to terminate the reaction. The absorbance of the reaction mixture at 450 nm was measured using a microplate reader (BioTek, Winooski, USA).

Co-immunoprecipitation (Co-IP) assay

Co-immunoprecipitation was performed using a Thermo Scientific Pierce co-IP kit according to the manufacturer's instructions. Whole cell lysate (WCL) was incubated overnight at 4 °C with A/G magnetic beads (B23202; Biotool) in Western/IP lysis buffer (Beyotime, Haimen, China). The immunoprecipitates were washed five times with Western/IP lysis buffer prior to IB. Samples were subjected to Western blot analysis using the following antibodies: anti-IgG (Proteintech, #30000-0-AP), anti-VDR (Abcam, #ab109234), anti-C-SRC (Proteintech, #11097-1-AP), anti-Y419-phospho-SRC (R&D, #DYC2685-2). IgG was regarded as a negative control.

Examination of red fluorescence protein (RFP)-LC3B puncta

To construct mRFP-LC3B-expressing cells, adenoviruses containing mRFP-LC3B coding sequences (Hanbio Biotechnology Co., Ltd, Shanghai, China) were transfected into the cells following the manufacturer's instructions. At 24 h after transfection, the cells were fixed with 4% formaldehyde for 15 min at room temperature. The number of red puncta was counted under a confocal microscope (Molecular Devices, ImageXpress Micro Confocal System). Six non-overlapping fields were observed, and at least 20 cells were counted in each group.

Immunohistochemical analysis

Formalin-fixed, paraffin-embedded liver tissues were sectioned to a thickness of 5 μm. The sections were then deparaffinized with xylene, hydrated using a graded alcohol series, and subjected to antigen retrieval and blocking. The sections were then incubated with anti-VDR antibodies (ab3508, 1:200), anti-cytokeratin19 antibody (ab76539, 1:200), anti-SQSTM1/P62 antibody (ab207305, 1:200) at 4 °C overnight followed by incubation with secondary antibodies. Immunoreactive signals were detected using 3,3′-diaminobenzidine and hematoxylin.

The expression of VDR and P62 protein were determined using a semiquantitative scoring method as described previously [35].

Establishment of the rhesus rotavirus (RRV)-induced BA mouse model [36]

Timed pregnant BALB/c mice were purchased from Guangdong Animal Experimental Center, China. Newborn pups (within 24 h of birth) were intraperitoneally injected with RRV (20 μL of 1.5×10^6 plaque-forming units/mL) or the same dose of saline. The neonatal pups were then divided into the following three groups: control group (10, regardless of sex), RRV group (15, regardless of sex), and RRV + 1,25-VD3 (15, regardless of sex, 1,25-VD3 50 μg/kg bodyweight once every other day). The weight, appearance, and survival of the mice were recorded daily. The extrahepatic bile ducts of the mice were examined using cholangiography. The mice were anesthetized with 0.5–2.5% isoflurane, dissected under a microscope on days 6 and 12, and blood and liver samples were collected for analysis. Following blood collection, euthanize the mice by inhalation of 4% isoflurane for 10 min. Autophagosome formation in extrahepatic bile duct epithelial cells (EBDECs) was observed by transmission electron microscopy (TEM). All experimental procedures involving animals were approved by the Institutional Animal Care and Use Committee of Laboratory Animal Center of Xi'an Jiaotong University.

Statistical analysis

All data are represented as mean ± standard error of the mean from three independent experiments. The correlations between the expression of VDR and clinicopathologic characteristics were evaluated using Chi-square tests. Means between two groups were compared using Student's t-test, while means between more than two groups were compared using one-way analysis of variance. All statistical analyses were performed in SPSS 22.0. Differences were considered significant at $p < 0.05$.

Supplementary Information

The online version contains supplementary material available at https://doi.org/10.1186/s12876-025-03640-5.

Supplementary Material 1

Acknowledgements

None.

Author contributions

Na Liu and Pu Zhao wrote the main manuscript text; Ping Cao, JunPeng Hui and YongKang Pan prepared figures and tables. Jiwen Cheng: Conceptualization; supervision; funding acquisition. All authors reviewed the manuscript.

Funding

The study was supported by the Key Research and Development plan of Shaanxi Province (Grant no. S2020-YF-YBSF-0245, 2021JQ-915) and Basic Scientific Research fee of Xi'an Jiaotong University (Grant no. xzy012019087, 2020YJ(ZYTS)495).

Data availability

Data can be requested from corresponding author.

Declarations

Ethics approval and consent to participate

The study was approved by the Ethics Committee of Xi'an Jiaotong University, and informed consent was obtained from the guardians of all children.

Consent for publication

Not applicable.

Competing interests

The authors declare no competing interests.

Author details

[1]Department of Pediatrics, First Affiliated Hospital of Xi'an Jiaotong University, Xi'an, Shaanxi Province 710061, China
[2]Department of Ultrasound, The Second Affiliated Hospital of Xi'an Jiaotong University, Xi'an, Shaanxi Province 710004, China
[3]Department of Neonatology, The Third Affiliated Hospital of Xi'an Jiaotong University, Xi'an, Shaanxi Province 710068, China
[4]Department of Pediatric Surgery, The Second Affiliated Hospital of Xi'an Jiaotong University, Xi'an, Shaanxi Province 710004, China
[5]Department of Pathology, Xi'an Children's Hospital, Xi'an, Shaanxi Province 710003, China
[6]Department of Neonatal Surgery, Xi'an Children's Hospital, Xi'an, Shaanxi Province 710003, China

Received: 29 August 2024 / Accepted: 21 January 2025
Published online: 29 January 2025

References

1. Bezerra JA, Wells RG, Mack CL, Karpen SJ, Hoofnagle JH, Doo E, Sokol RJ. Biliary atresia: clinical and Research challenges for the twenty-First Century. Hepatology. 2018;68(3):1163–73.
2. Malik A, Thanekar U, Mourya R, Shivakumar P. Recent developments in etiology and disease modeling of biliary atresia: a narrative review. Dig Med Res. 2020;3:59.
3. Sun S, Xu M, Zhuang P, Chen G, Dong K, Dong R, Zheng S. Effect and mechanism of vitamin D activation disorder on liver fibrosis in biliary atresia. Sci Rep. 2021;11(1):19883.
4. Zhuang P, Sun S, Dong R, Chen G, Huang Y, Zheng S. Associations between Vitamin D and liver function and liver fibrosis in patients with biliary atresia. Gastroenterol Res Pract. 2019;2019:4621372.
5. Ding N, Yu RT, Subramaniam N, Sherman MH, Wilson C, Rao R, Leblanc M, Coulter S, He M, Scott C, et al. A vitamin D receptor/SMAD genomic circuit gates hepatic fibrotic response. Cell. 2013;153(3):601–13.
6. Gascon-Barré M, Demers C, Mirshahi A, Néron S, Zalzal S, Nanci A. The normal liver harbors the vitamin D nuclear receptor in nonparenchymal and biliary epithelial cells. Hepatology. 2003;37(5):1034–42.
7. D'Aldebert E, Biyeyeme Bi Mve MJ, Mergey M, Wendum D, Firrincieli D, Coilly A, Fouassier L, Corpechot C, Poupon R, Housset C, et al. Bile salts control the antimicrobial peptide cathelicidin through nuclear receptors in the human biliary epithelium. Gastroenterology. 2009;136(4):1435–43.
8. Firrincieli D, Zúñiga S, Rey C, Wendum D, Lasnier E, Rainteau D, Braescu T, Falguières T, Boissan M, Cadoret A, et al. Vitamin D nuclear receptor deficiency promotes cholestatic liver injury by disruption of biliary epithelial cell junctions in mice. Hepatology. 2013;58(4):1401–12.
9. Madadi-Sanjani O, Petersen C. Translational Research in biliary atresia: news from mice and men. Eur J Pediatr Surg. 2019;29(4):336–41.
10. Vij M, Rela M. Biliary atresia: pathology, etiology and pathogenesis. Future Sci OA. 2020;6(5):FSO466.

11. Wang J, Xu Y, Chen Z, Liang J, Lin Z, Liang H, Xu Y, Wu Q, Guo X, Nie J, et al. Liver Immune Profiling reveals Pathogenesis and therapeutics for biliary atresia. Cell. 2020;183(7):1867–e188326.
12. Chusilp S, Lee C, Li B, Lee D, Yamoto M, Ganji N, Vejchapipat P, Pierro A. A novel model of injured liver ductal organoids to investigate cholangiocyte apoptosis with relevance to biliary atresia. Pediatr Surg Int. 2020;36(12):1471–9.
13. Buitrago C, Boland R. Caveolae and caveolin-1 are implicated in 1alpha, 25(OH)2-vitamin D3-dependent modulation of src, MAPK cascades and VDR localization in skeletal muscle cells. J Steroid Biochem Mol Biol. 2010;121(1–2):169–75.
14. Asai A, Miethke A, Bezerra JA. Pathogenesis of biliary atresia: defining biology to understand clinical phenotypes. Nat Rev Gastroenterol Hepatol. 2015;12(6):342–52.
15. Harada K, Sato Y, Isse K, Ikeda H, Nakanuma Y. Induction of innate immune response and absence of subsequent tolerance to dsRNA in biliary epithelial cells relate to the pathogenesis of biliary atresia. Liver Int. 2008;28(5):614–21.
16. Ichimiya T, Yamakawa T, Hirano T, Yokoyama Y, Hayashi Y, Hirayama D, Wagatsuma K, Itoi T, Nakase H. Autophagy and autophagy-related diseases: a review. Int J Mol Sci. 2020;21(23):8974.
17. Jee SC, Cheong H. Autophagy/Mitophagy regulated by Ubiquitination: a promising pathway in Cancer therapeutics. Cancers (Basel). 2023;15(4):1112.
18. Nakanuma Y, Sasaki M, Harada K. Autophagy and senescence in fibrosing cholangiopathies. J Hepatol. 2015;62(4):934–45.
19. Nakajima Y, Yamazaki Y, Gao X, Hashimoto M, Nio M, Wada M, Fujishima F, Sasano H. Association between mitochondrial and nuclear DNA damages and cellular senescence in the patients with biliary atresia undergoing Kasai portoenterostomy and liver transplantation. Med Mol Morphol. 2022;55(2):131–45.
20. Qian H, Chao X, Williams J, Fulte S, Li T, Yang L, Ding WX. Autophagy in liver diseases: a review. Mol Aspects Med. 2021;82:100973.
21. Ismailova A, White JH. Vitamin D, infections and immunity. Rev Endocr Metab Disord. 2022;23(2):265–77.
22. Kempinska-Podhorodecka A, Milkiewicz M, Wasik U, Ligocka J, Zawadzki M, Krawczyk M, Milkiewicz P. Decreased expression of vitamin D receptor affects an Immune response in primary biliary cholangitis via the VDR-miRNA155-SOCS1 pathway. Int J Mol Sci. 2017;18(2):289.
23. Berridge MJ. Vitamin D deficiency accelerates ageing and age-related diseases: a novel hypothesis. J Physiol. 2017;595(22):6825–36.
24. Dos Santos M, de Souza Silva JM, Bartikoski BJ, Freitas EC, Busatto A, do Espírito Santo RC, Monticielo OA, Xavier RM. Vitamin D supplementation modulates autophagy in the pristane-induced lupus model. Adv Rheumatol. 2022;62(1):27.
25. Lan T, Yan B, Guo W, Shen Z, Chen J. VDR promotes nucleus pulposus cell mitophagy as a protective mechanism against oxidative stress injury. Free Radic Res. 2022;56(3–4):316–27.
26. Chen HY, Chiu LC, Yek YL, Chen YL. Detecting rickets in premature infants and treating them with calcitriol: experience from two cases. Kaohsiung J Med Sci. 2012;28(8):452–6.
27. Qiu Y, Yang J, Wang W, Zhao W, Peng F, Xiang Y, Chen G, Chen T, Chai C, Zheng S, et al. HMGB1-promoted and TLR2/4-dependent NK cell maturation and activation take part in rotavirus-induced murine biliary atresia. PLoS Pathog. 2014;10(3):e1004011.
28. Azagra-Boronat I, Massot-Cladera M, Knipping K, Van't Land B, Tims S, Stahl B, Knol J, Garssen J, Franch À, Castell M, et al. Oligosaccharides modulate Rotavirus-Associated Dysbiosis and TLR Gene expression in neonatal rats. Cells. 2019;8(8):876.
29. Chen Y, Lin J, Zhao Y, Ma X, Yi H. Toll-like receptor 3 (TLR3) regulation mechanisms and roles in antiviral innate immune responses. J Zhejiang Univ Sci B. 2021;22(8):609–32.
30. Zang R, Lian H, Zhong X, Yang Q, Shu HB. ZCCHC3 modulates TLR3-mediated signaling by promoting recruitment of TRIF to TLR3. J Mol Cell Biol. 2020;12(4):251–62.
31. Beesabathuni NS, Park S, Shah PS. Quantitative and temporal measurement of dynamic autophagy rates. Autophagy. 2023;19(4):1164–83.
32. Plesa M, Gaudet M, Mogas A, Jalaleddine N, Halayko A, Al Heialy S, Hamid Q. Vitamin D3 attenuates viral-Induced inflammation and fibrotic responses in bronchial smooth muscle cells. Front Immunol. 2021;12:715848.
33. Li Y, Si H, Ma Y, Li S, Gao L, Liu K, Liu X. Vitamin D3 affects the gut microbiota in an LPS-stimulated systemic inflammation mouse model. Microbes Infect. 2023;25(8):105180.
34. Verscheijden LFM, van der Zanden TM, van Bussel LPM, de Hoop-Sommen M, Russel FGM, Johnson TN, de Wildt SN. Chloroquine Dosing recommendations for Pediatric COVID-19 supported by modeling and Simulation. Clin Pharmacol Ther. 2020;108(2):248–52.
35. Cheng J, Chen Y, Zhao P, Liu X, Dong J, Li J, Huang C, Wu R, Lv Y. Downregulation of miRNA-638 promotes angiogenesis and growth of hepatocellular carcinoma by targeting VEGF. Oncotarget. 2016;7(21):30702–11.
36. Zhang R, Su L, Fu M, Wang Z, Tan L, Chen H, Lin Z, Tong Y, Ma S, Ye R, et al. CD177 + cells produce neutrophil extracellular traps that promote biliary atresia. J Hepatol. 2022;77(5):1299–310.

Publisher's note